Supplementary information

The investigation of $Ni(OH)_2$/Ni as anode for high performance Li-ion battery

Shibing Ni [*a], Xiaohu Lv[a], Tao Li[a], Xuelin Yang[*a], and Lulu Zhang

[a] College of Mechanical and Material Engineering, Three Gorges University, 8 Daxue Road, Yichang 443002, PR China

Experiments

Ni foam (100 PPI pore size, 380 g m^{-2} surface density, 1.5 mm thick) was purchased from Changsha Lyrun New Material corporation. In a typical procedure, Ni foam were ultrasonically washed with distilled water and ethanol, and then added into 50 ml teflonlined autoclave. Distilled water was subsequently added to 80% of its capacity. The autoclave was sealed and placed in an oven, heated at 120 °C for 24 h. After the reaction, the autoclave was cooled in air. The resulting Ni foam finally was dried in an oven at 70 °C for 24 h. $Ni(OH)_2$ powers were obtained by a hydrothermal method: 2.5 mmol nickelous acetate and 2.5 mmol sodium hydroxide were dissolved in 30 ml distilled water. After stirring for 20 minutes, the homogeneous green solution was transferred into a 50 ml teflonlined autoclave, distilled water was subsequently added to 80% of its capacity. The autoclave was at last sealed and placed in an oven, heated at 120 ^oC for 24 h. For measuring the weight of $Ni(OH)_2$ on Ni foam, $Ni(OH)_2$/Ni foam (3 cm×2.4 cm) were annealed in N_2 atmosphere at 300 ^oC for 5h

* Corresponding author. fax: +86 717 6397559. E-mail address: shibingni07@gmail.com
* xlyang@ctgu.edu.cn

(heating rate of 3 ^{o}C/min). According to the reaction ($Ni(OH)_2 \rightarrow NiO + H_2O$), the weight of $Ni(OH)_2$ on Ni foam can be estimated. $m_{Ni(OH)_2} = \Delta m \times 92.7/18$, where Δm is the weight difference of $Ni(OH)_2$/Ni before and after annealing in N_2 atmosphere. The weight of $Ni(OH)_2$ on $Ni(OH)_2$/Ni disk electrode can be further calculated according to the area of the electrode.

The structure and morphology of the resulting products were characterized by X-Ray powder diffraction (Rigaku Ultima IV Cu Kα radiation λ=1.5406 Å), field-emission scanning electron microscopy (FE-SEM JSM 7500F, JEOL), and transmission electron microscopy (TEM JEM-2100) equipped with selected area electron diffraction (SAED). For fabricating of lithium ion battery, the as-prepared Ni foam discs were dried (120 ^{o}C, 24 h, vacuum). Coin-type cells (2025) of Li/1 M $LiPF_6$ in ethylene carbonate, dimethyl carbonate and diethyl carbonate (EC/DMC/DEC, 1:1:1 v/v/v)/Ni foam discs with diameter of 14 mm were assembled in an argon-filled dry box (MIKROUNA, Super 1220/750, H_2O<1.0 ppm, O_2<1.0 ppm). A Celgard 2400 microporous polypropylene was used as the separator membrane. The cells were tested in the voltage range between 0.02 and 3 V with a multichannel battery test system (LAND CT2001A). The Cyclic voltammetry (CV) measurement of the electrodes was carried out on a CHI660C electrochemical workstation at a scan rate of 0.1 mV s^{-1} between 0 and 3 V.

We measured the pH value of the autoclave before and after hydrothermal reaction, and we found the value shows no obvious variation before and after reaction.

Considering the experimental results, we propose the formation of $Ni(OH)_2$ is likely due to an electrochemical corrosion process as follows:

$$Ni + n\ H_2O \rightarrow [Ni(H_2O)_n]^{2+} + 2e^- \quad (1)$$

$$O_2 + 2\ H_2O + 4\ e^- \rightarrow 4\ OH^- \quad (2)$$

$$[Ni(H_2O)_n]^{2+} + 2\ OH^- \rightarrow Ni(OH)_2 + n\ H_2O \quad (3)$$

In addition, the formation of nanoflake morphology is relevant to the intrinsic crystal structure of β-$Ni(OH)_2$. β-$Ni(OH)_2$ is one kind of typical hydrotalcite-like compounds. In hydrotalcite-like compounds, the alkaline layered hydroxide has a hexagonal close packing of hydroxyl ions, where each divalent metal ion is octahedron sharing their edges to form 2D brucite-like flakes which then stack upon one another to form a layered solid via various interlayer chemical interactions [1, 2]. As a result, under normal reaction condition, such compounds easily present the thin flake-like crystallite morphology with the flake surface perpendicular to the c-axis of crystal.

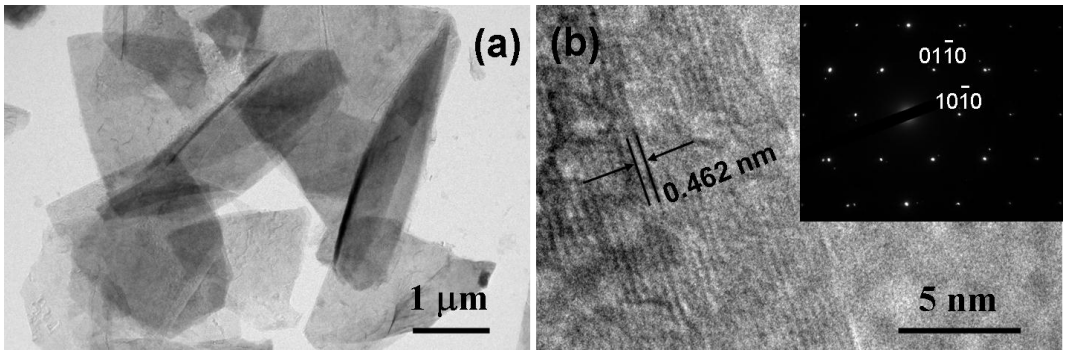

Fig. S1 TEM (a) and HR-TEM (b) images of the $Ni(OH)_2$. The insert of Fig. S1(b) is the SAED pattern.

TEM image is shown in fig. S1(a), from which flake-like morphology of $Ni(OH)_2$ with mean size about 3 μm can be clearly observed. Fig. S1(b) is a high resolution TEM (HR-TEM) image of the $Ni(OH)_2$ nanoflake, which shows clear lattice fringes.

The interplanar spacing is about 0.462 nm, which corresponds to the (001) plane of hexagonal β-$Ni(OH)_2$. The results are in accordance with the proposed formation mechanism of β-$Ni(OH)_2$ nanoflake. The insert of fig. S1(b) is the selected area electron diffraction pattern (SAED) of the β-$Ni(OH)_2$ nanoflake, regular diffraction spots suggest the nanoflakes are well crystallized.

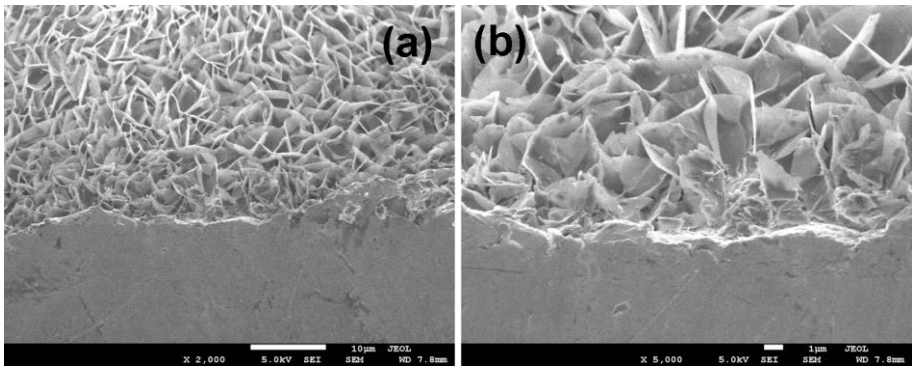

Fig. S2. Oblique view SEM images of $Ni(OH)_2$ film with low (a) and high (b) magnification.

As shown in Fig. S2, SEM images of $Ni(OH)_2$/Ni with oblique view reveal the thickness of $Ni(OH)_2$ film on Ni is about 3 μm, which is in accordance with the size of $Ni(OH)_2$ nanoflakes, suggesting a single layer growth of $Ni(OH)_2$.

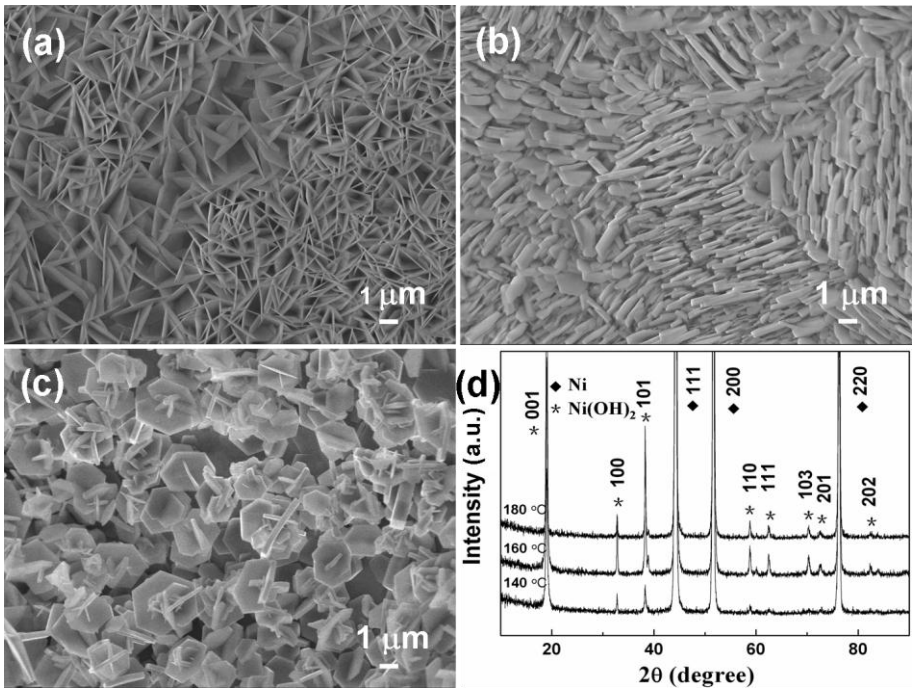

Fig. S3 SEM images (a)-(c) and XRD patterns (d) of $Ni(OH)_2$ on Ni foam obtained at different temperature. (a) 140 ^oC, (b) 160 ^oC and (c) 180 ^oC.

As shown in Fig. S3, the morphology of $Ni(OH)_2$ on Ni foam can be simply tuned by changing the temperature of hydrothermal reaction. Fig. S3(a) is the SEM image of the $Ni(OH)_2$ obtained at 140 ^oC for 24h, showing flake-like morphology with mean thickness of 100 nm. When applying a temperature of 160 ^oC, micro-sized $Ni(OH)_2$ sheets with mean thickness about 500 nm were obtained, which is shown in Fig. S3(b). When the temperature arriving at 180 ^oC, micro-sized $Ni(OH)_2$ plates were obtained. As shown in Fig. S3(c), the mean size and mean thickness of those plates is about 2 μm and 250 nm, respectively. The XRD patterns of the products were shown in Fig. S3(d), which are in good agreement with β-$Ni(OH)_2$ (JCPDS, No. 74-2075), showing no phase variation along with the reaction temperature.

The XRD patterns of both $Ni(OH)_2$/Ni and $Ni(OH)_2$ powder after annealing were

characterized. As shown in Fig. S4(a)-(c), after annealing (the annealing process was carried out under a very low heating rate of 3 ^{o}C/min), no diffraction peaks of $Ni(OH)_2$ for both samples were observed, which suggest the totally decomposition of $Ni(OH)_2$. The thermal behavior of $Ni(OH)_2$/Ni was investigated by means of TG/DSC measurement in N_2 atmosphere at a heating rate of 5 K min^{-1}. As shown in Fig. S4(d), the DSC curve shows a small endothermic peak at 70 ^{o}C and a big endothermic peak at 290 ^{o}C, which correspond to the elimination of adsorbed water and the decomposition of $Ni(OH)_2$ into NiO. It can be seen that the corresponding weight loss in the TG curve for the first endothermic process is not visible, suggesting the mass of adsorbed water is very small and can be nearly ignored. In addition, the weight of the $Ni(OH)_2$/Ni before and after annealing was measured under the same condition (air atmosphere and room temperature). Considering the TG and DSC results and above mentions, we suggest the weight of $Ni(OH)_2$ on Ni foam can be calculated by $m_{Ni(OH)2} = \Delta m \times 92.7/18$, where Δm is the weight difference of $Ni(OH)_2$/Ni before and after annealing in N_2 atmosphere.

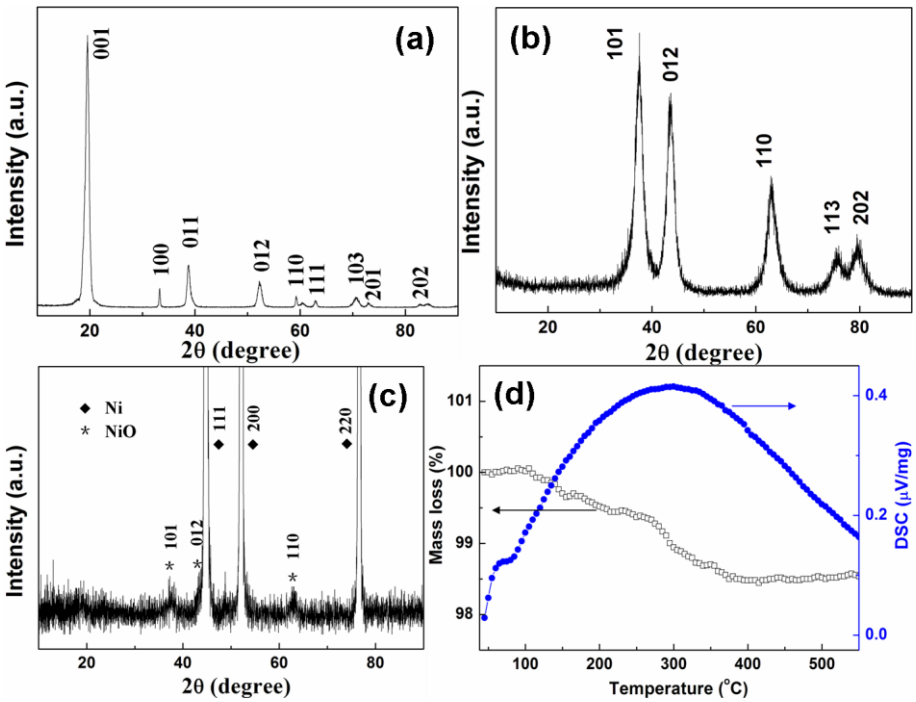

Fig. S4 XRD patterns of β-$Ni(OH)_2$ powder before (a) and after (b) annealing in N_2 at 300 ^{o}C for 5h. (c) XRD pattern of $Ni(OH)_2$ nanowall/Ni foam after annealing in N_2 at

300 ^{o}C for 5h. (d) TG and DSC curves for $Ni(OH)_2$ nanowall/Ni foam.

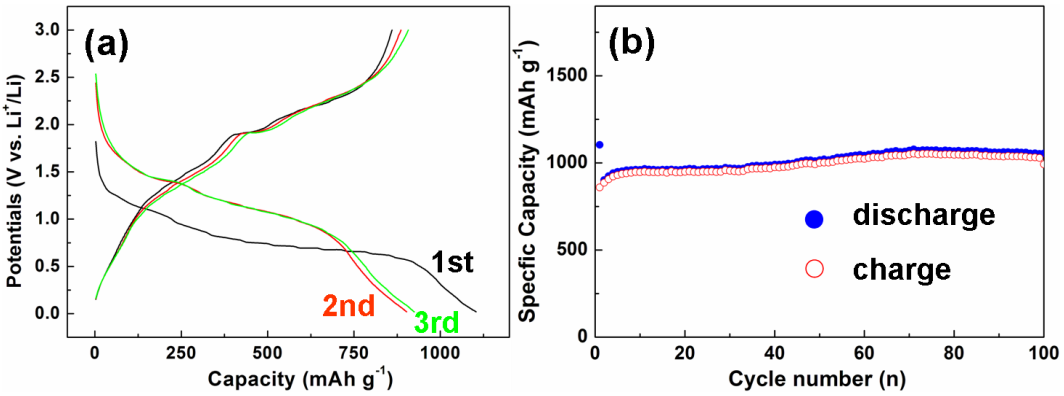

Fig. S5 The initial three charge and discharge curves (a) and cycle performance (b) of the $Ni(OH)_2$ nanowalls electrode.

As shown in Fig. S5, the initial discharge capacity of the as-synthesized $Ni(OH)_2$ nanowalls electrode is about 1103 mAh g^{-1}, which is lower than the initial discharge capacity of $Ni(OH)_2$ and reduced graphite oxide composite electrode. However, the cycle stability of $Ni(OH)_2$ nanowalls electrode is much improved than that of $Ni(OH)_2$ and reduced graphite oxide composite [3], maintaining of discharge capacity of 1054 mAh g^{-1} after 100 cycles. The capacity of the $Ni(OH)_2$ nanowalls electrode is much higher than the theoretical capacity of $Ni(OH)_2$ based on the reaction $Ni(OH)_2 + 2e^- + 2Li^+ \leftrightarrow 2LiOH + Ni$ (578 mAh g^{-1}), which can be ascribed to the reversible growth of a polymeric gel-like film resulting from kinetically activated electrolyte degradation [4, 5]. This is in accordance with CV curves with symmetrical reduction and oxidation peaks.

For comparison, the electrochemical performance of $Ni(OH)_2$ powers was studied. As shown in Fig. S6, the $Ni(OH)_2$ power electrode shows initial discharge capacity of

1048 mAh g^{-1}. The capacity decreases sharply along with the increasing of cycle number, after 100 cycles, the discharge capacity is less than 50 mAh g^{-1}. The initial discharge capacity of $Ni(OH)_2$ nanowalls electrode is close to that of $Ni(OH)_2$ powder, but the cycling performance is much better than that of $Ni(OH)_2$ powder.

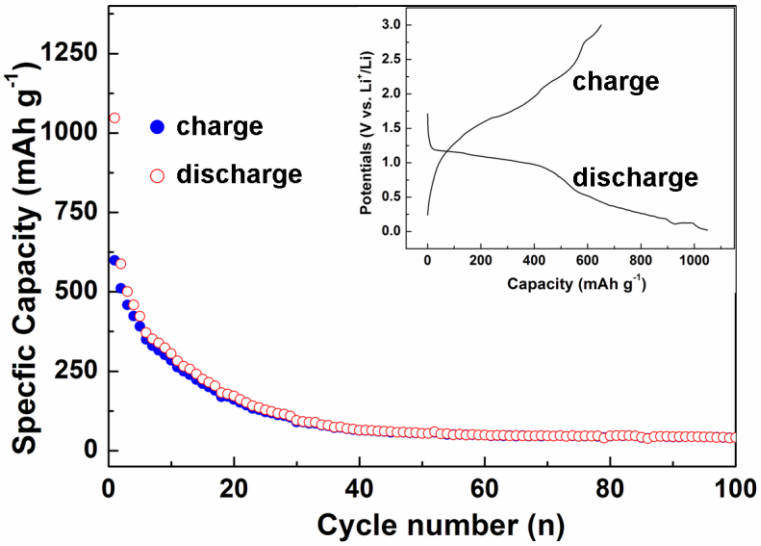

Fig. S6 cycle performance of $Ni(OH)_2$ powder electrode. The insert is the initial charge and discharge curve.

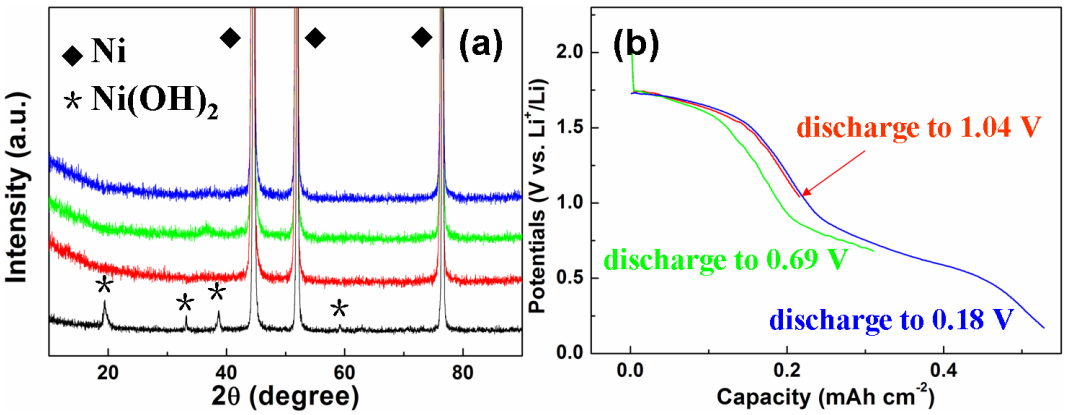

Fig. S7 XRD patterns (a) and discharge curves (b) of $Ni(OH)_2$ nanowalls electrode under different discharge state.

For studying the reaction mechanism, we systematically and repeatedly measured the XRD pattern of $Ni(OH)_2$ under different charge and discharge state under a low san

rate of 2^{o} min^{-1}. Fig. S7(a) is the XRD patterns of $Ni(OH)_2$/Ni electrode under different discharge potential (black for the as-synthesized $Ni(OH)_2$/Ni, red for discharging to 1.04 V, green for discharging to 0.69 V, blue for discharging to 0.18 V). As seen, no diffraction peaks of $Ni(OH)_2$ can be observed under different discharge potential, which suggests the disappearance of $Ni(OH)_2$ phase owing to the electrochemical reactions between $Ni(OH)_2$ and electrolyte. The corresponding discharge curves are shown in Fig. S7(b), different sloping potential ranges suggest that different electrochemical reactions occurs under different discharge potential. No obvious diffraction peaks of other phase are detected, which may be due to the formation of intermedial amorphous phase.

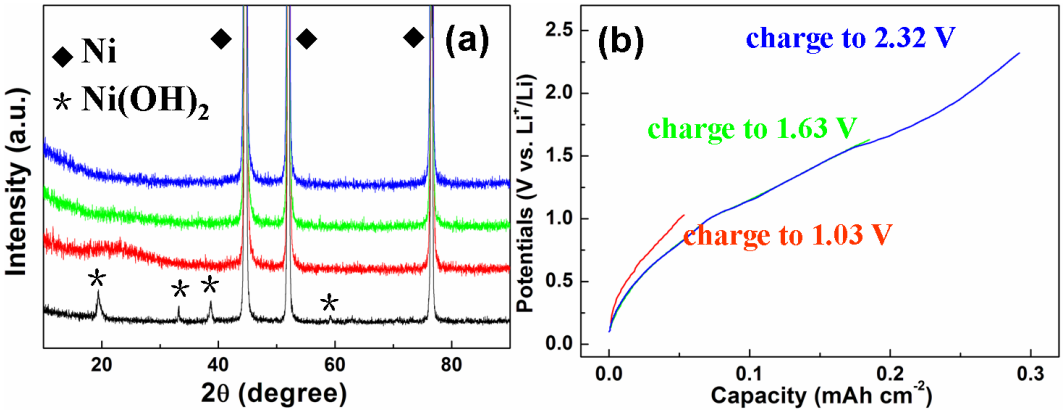

Fig. S8 XRD patterns (a) and charge curves (b) of $Ni(OH)_2$ nanowalls electrode under different charge state.

Fig. S8(a) is the XRD patterns of $Ni(OH)_2$/Ni electrode under different charge potential (black for the as-synthesized $Ni(OH)_2$/Ni, red for charging to 1.03 V, green for discharging to 1.63 V, blue for discharging to 2.32 V). The corresponding charge curves are shown in Fig. 8(b), different charge potential ranges suggest different electrochemical reactions between the electrode and electrolyte. As seen, no

diffraction peaks of $Ni(OH)_2$ were observed in the whole charging process, which indicates the formation of amorphous phase due to the electrochemical reactions.

[1] Y.Y. Luo, G.T. Duan and G.H. Li, J. Solid State Chem. 2007, **180,** 2149-2153.

[2] Z.H. Liang, Y.J. Zhu and X.L. Hu, J. Phys. Chem. B 2004, **108,** 3488-3491.

[3] B.J. Li, H.Q. Cao, J. Shao, H. Zheng, Y.X. Lu, J.F. Yin and M.Z. Qu, Chem. Commun. 2011, **47,** 3159-3161.

[4] S. Grugeon, S. Laruelle, L. Dupont and J. M. Tarascon, Solid State Sci. 2003, **5**, 895-904.

[5] G. Zhou, D.W. Wang, F. Li, L. Zhang, N. Li, Z.S. Wu, L. Wen, G.Q. Lu and H.M. Cheng, Chem. Mater., 2010, **22,** 5306-5313.